Enantioselective chiral orientation induced by a combination of a long and a short laser pulse

Long Xu [*]

AMOS and Department of Chemical and Biological Physics, The Weizmann Institute of Science, Rehovot 7610001, Israel

Enantioselective orientation of chiral molecules excited by a shaped picosecond laser pulse and a delayed femtosecond pulse is considered. Using quantum-mechanical simulations, we demonstrate a strong field-free enantioselective orientation along the laser propagation direction. In addition, we use a classical model to reproduce the enantioselective orientation. Moreover, the analysis of the corresponding classical system allows understanding the qualitative features of the induced enantioselective orientation. The strong enantioselective orientation may be used for the separation of chiral enantiomers using inhomogeneous electrostatic fields.

I. INTRODUCTION

Chiral molecules exist in two species: left- and right-handed enantiomers. These enantiomers are mirror images of each other, and they cannot be superimposed on each other by translations and rotations [1]. Since its discovery by Pasteur in 1848 [2], the phenomenon of molecular chirality has gained immense importance in biology, physics, chemistry, and the pharmaceutical industry. Various methods for chiral discrimination have been proposed and implemented over the years. Examples involving laser fields include photoelectron circular dichroism [3–7], microwave three-wave mixing spectroscopy [8–15], Coulomb explosion imaging [16–18], high-order-harmonic generation [19], and enantiospecific interaction with achiral magnetic substrates [20].

In the last few years, the enantioselective orientation of chiral molecules excited by laser pulses with twisted polarization has been investigated [21–26]. Examples of fields with twisted polarization include delayed cross-polarized laser pulses [27–29], the optical centrifuge for molecules [30–34], chiral pulse trains [35,36], and polarization-shaped pulses [37–41]. In addition, it was theoretically shown that terahertz (THz) pulses with twisted polarization [42] and two-color laser pulses [43,44] are effective for inducing enantioselective orientation.

When molecules are exposed to linearly polarized nonresonant laser fields, the most polarizable molecular axis tends to align along the polarization direction. When molecules are excited by laser pulses with twisted polarization, the most polarizable molecular axis tends to follow the rotating polarization vector, resulting in unidirectional rotation [27–29,45–47]. Furthermore, in the case of chiral molecules, such twisted fields induce an orienting torque along the most polarizable axis [22,23]. This additional torque enantioselectively orients the chiral molecules perpendicular to the plane of polarization twisting. The orientation direction (along or against the laser propagation direction) depends on the sense of twisting and the handedness of the molecule.

In this paper, we study the orientation of chiral molecules excited by a linearly polarized shaped picosecond laser pulse [48–52] and a delayed copropagating cross-polarized femtosecond pulse. A slowly rising and sharply truncated picosecond pulse is used to produce a highly aligned molecular state. With long pulses, a high degree of alignment can be reached without significant molecular ionization. Achieving the same degree of alignment with a femtosecond laser pulse would require a much higher peak power, which inevitably results in sizable molecular ionization. After the shaped picosecond pulse is suddenly switched off, a cross-polarized femtosecond laser pulse is applied, leading to enantioselective orientation along a direction perpendicular to the plane of polarization twisting, that is, along the propagation direction of the pulses. The highly aligned state induced by the picosecond pulse enables a high degree of enantioselective orientation. A classical model reproduces well the enantioselective orientation and is used to analyze the various qualitative features of the effect, including the vanishing orientation along any direction in the plane of laser polarizations, the enantioselective orientation along the laser propagation direction, and the roles played by the picosecond and femtosecond laser pulses.

II. NUMERICAL METHODS

For the quantum-mechanical simulations, we consider the chiral molecule to be a rigid rotor. The Hamiltonian describing the molecular rotation driven by the laser field is given by $H(t) = H_r + H_{\text{int}}(t)$ [53,54], where H_r is the field-free Hamiltonian and $H_{\text{int}}(t) = -\mathbf{E} \cdot (\boldsymbol{\alpha}\mathbf{E})/2$ is the interaction of the molecule with the laser field. Here, $\boldsymbol{\alpha}$ is the molecular polarizability tensor, and $\mathbf{E}$ is the external electric field. The wave function is expressed in the basis of field-free symmetric-top eigenfunctions $|JKM\rangle$ [55]. Here, J is the total angular momentum, while K and M are its projections on the molecule-fixed z and laboratory-fixed Z axes respectively. The
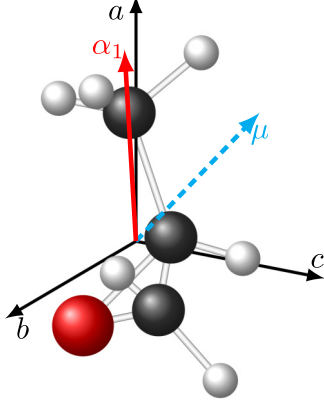
---
[*]long.xu@weizmann.ac.il

FIG. 1. Right-handed propylene oxide molecule. Axes a, b, and c are the principal axes of the inertia tensor. Atoms are color coded: black, carbon; gray, hydrogen; red, oxygen. The dashed blue and solid red arrows represent the dipole moment (see Table I) and $\boldsymbol{\alpha}_1$ axis, $\boldsymbol{\alpha}_1 = (0.293, 0.115, 0.949)$, respectively.

nonzero matrix elements of the field-free Hamiltonian are [55]

$$\langle JKM|H_r|JKM \rangle = \frac{B+C}{2}[J(J+1) - K^2] + AK^2,$$

$$\langle JKM|H_r|J, K \pm 2, M \rangle = \frac{B-C}{4}f(J, K \pm 1), \quad (1)$$

where $f(J, K) = \sqrt{(J^2 - K^2)[(J+1)^2 - K^2]}$, $A = \hbar^2/2I_a$, $B = \hbar^2/2I_b$, and $C = \hbar^2/2I_c$, with the moments of inertia $I_a < I_b < I_c$. The time-dependent Schrödinger equation $i\hbar\partial_t|\Psi(t)\rangle = H(t)|\Psi(t)\rangle$ is solved by numerical exponentiation of the Hamiltonian matrix (see EXPOKIT [56]). Thermal effects are included by considering the different initial states with the relative weight given by the Boltzmann distribution. A detailed description of our numerical scheme can be found in [25].

III. STRONG ENANTIOSELECTIVE ORIENTATION

Here, we consider the propylene oxide molecule (PPO, CH_3CHCH_2O) as a typical example of a chiral molecule. The right-handed propylene oxide molecule is shown in Fig. 1. Table I summarizes the molecular properties of (R)-PPO (the right-handed enantiomer), which were computed using the GAUSSIAN software package (method: density functional theory within the CAM-B3LYP/aug-cc-pVTZ scheme) [57]. The molecules are excited by a shaped picosecond laser pulse followed by a femtosecond laser pulse. The picosecond laser

TABLE I. Molecular properties of the (R)-PPO molecule: moments of inertia (in atomic units), elements of the dipole moment (in debyes), and polarizability tensors (in atomic units) expressed in the frame of principal axes of inertia.

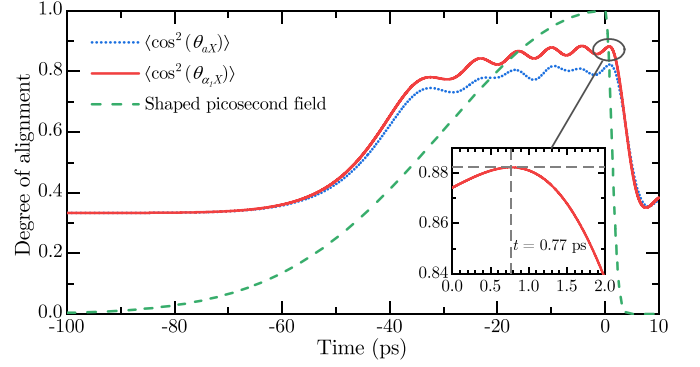| Moments of inertia	Dipole components	Polarizability components
$I_a = 180386$	$\mu_a = 0.965$	$\alpha_{aa} = 45.63, \alpha_{ab} = 2.56$
$I_b = 493185$	$\mu_b = -1.733$	$\alpha_{bb} = 37.96, \alpha_{ac} = 0.85$
$I_c = 553513$	$\mu_c = 0.489$	$\alpha_{cc} = 37.87, \alpha_{bc} = 0.65$

FIG. 2. Quantum-mechanically calculated time-dependent degree of molecular alignment along the polarization direction of the picosecond pulse. The initial temperature is 0 K. Note that the degrees of alignment for the two enantiomers, (R)- and (S)-PPO, are the same. The dashed green line represents the envelope of the shaped picosecond field [see Eq. (2)]. The inset shows the magnified portion of $\langle \cos^2(\theta_{\alpha_1 X}) \rangle$.

pulse is polarized along the laboratory-fixed X axis, and it is used to produce a highly aligned molecular state, while the femtosecond laser pulse, polarized in the XY plane at angle $\pi/4$ to the polarization of the picosecond pulse, is used to induce the enantioselective orientation. Such laser pulses with twisted polarization induce a unidirectional molecular rotation in the XY plane, allowing us to define a unique Z direction using the right-hand rule. Both pulses propagate in the same direction, the Z direction. The electric field of the shaped picosecond laser pulse (see Fig. 2) is given by

$$\mathbf{E}^p(t) = E_0^p \exp\left(-2\ln 2\frac{t^2}{\sigma^2}\right)\cos(\omega t)\mathbf{e}_X, \quad (2)$$

where

$$\begin{cases} \sigma = \sigma_{\text{on}}, & t < 0, \\ \sigma = \sigma_{\text{off}}, & t \geqslant 0. \end{cases}$$

The electric field of the femtosecond laser pulse is

$$\mathbf{E}^f(t) = \frac{E_0^f}{\sqrt{2}} \exp\left[-2\ln 2\frac{(t-\tau)^2}{\sigma_f^2}\right]\cos(\omega t)(\mathbf{e}_X + \mathbf{e}_Y). \quad (3)$$

Here, E_0^p (E_0^f) is the peak amplitude of the picosecond (femtosecond) field, ω is the carrier frequency, and $\mathbf{e}_X$ ($\mathbf{e}_Y$) is a unit vector along the laboratory X (Y) axis. σ_{on} and σ_{off} represent the FWHM of the slow switch on and the rapid switch off, respectively. σ_f is the FWHM of the femtosecond laser pulse, and τ is defined as the time at which the femtosecond laser pulse is applied.

Figure 2 shows the time-dependent degree of alignment, quantified by the average of the squares of the directional cosines, $\langle \cos^2(\theta_{aX}) \rangle(t) = \langle \Psi(t)|(\mathbf{a} \cdot \mathbf{e}_X)^2|\Psi(t)\rangle$ and $\langle \cos^2(\theta_{\alpha_1 X}) \rangle(t) = \langle \Psi(t)|(\boldsymbol{\alpha}_1 \cdot \mathbf{e}_X)^2|\Psi(t)\rangle$. $\mathbf{a} = (0, 0, 1)$ is the molecule-fixed a axis, while $\boldsymbol{\alpha}_1$ is the most polarizable molecular axis, and for the (R)-PPO molecule, $\boldsymbol{\alpha}_1 = (0.293, 0.115, 0.949)$ (see Fig. 1). The vectors are expressed in the molecule-fixed frame using the basis consisting of the three inertia principal axes b, c, a, namely, $x \to b$, $y \to c$, $z \to a$, such that an arbitrary vector $\mathbf{r}$ has Cartesian compo-
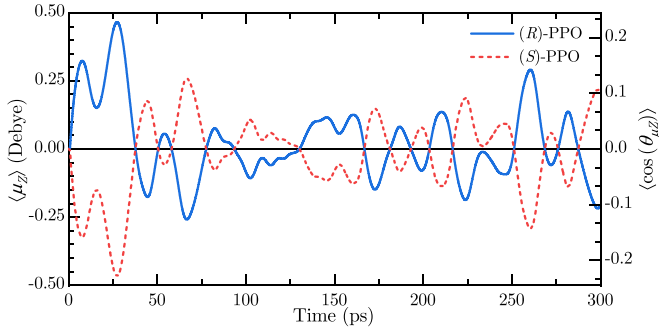
FIG. 3. Quantum expectation value of the Z projection of the dipole signal $\langle \mu_Z \rangle (t)$ or the degree of orientation $\langle \cos (\theta_{\mu Z}) \rangle \equiv \langle \mu_Z \rangle (t) / \mu$. Here, $\theta_{\mu Z}$ is the angle between the molecular dipole moment and the laboratory Z axis; μ is the magnitude of the dipole moment. (R)- and (S)-PPO denote the right- and left-handed enantiomers of the PPO molecule, respectively. Note that the signals are π out of phase for the two enantiomers.

nents $\mathbf{r} = (r_b, r_c, r_a)$ in the molecule-fixed frame. θ_{aX} ($\theta_{\alpha_1 X}$) denotes the angle between the molecule-fixed a (α_1) axis and the laboratory-fixed X axis (the polarization direction of the picosecond pulse). Here, the initial state is the ground rotational state (temperature is 0 K). The peak intensity of the picosecond laser pulse is $I^p = 10^{12}\,\mathrm{W/cm^2}$; the FWHMs are $\sigma_{\mathrm{on}} = 50\,\mathrm{ps}$ and $\sigma_{\mathrm{off}} = 2\,\mathrm{ps}$. In the presence of the picosecond pulse, the most polarizable molecular α_1 axis is aligned along the polarization direction. Figure 2 shows high degrees of alignment of the molecular a and α_1 axes building up during the picosecond laser pulse. The maximal degrees of alignment are $\langle \cos^2 (\theta_{aX}) \rangle \simeq 0.82$ and $\langle \cos^2 (\theta_{\alpha_1 X}) \rangle \simeq 0.88$.

During the turn-off stage of the shaped picosecond pulse, around the time when the degree of alignment is at maximum (see the inset in Fig. 2), a cross-polarized femtosecond laser pulse is applied. The femtosecond laser pulse is polarized at angle $\pi/4$ to the X axis. The peak intensity of the femtosecond laser pulse is $I^f = 10^{13}\,\mathrm{W/cm^2}$, its FWHM is $\sigma_f = 0.1\,\mathrm{ps}$, and $\tau = 0.77\,\mathrm{ps}$ [see Eq. (3)]. Figure 3 shows the time-dependent dipole signal along the laboratory Z axis, $\langle \mu_Z \rangle (t) = \langle \Psi(t) | \boldsymbol{\mu} \cdot \mathbf{e}_Z | \Psi(t) \rangle$ ($\boldsymbol{\mu}$ is the permanent dipole moment). As expected, shortly after the pulse, enantioselective orientation along the laser propagation direction appears; namely, the sign of $\langle \mu_Z \rangle (t)$ is positive (negative) for (R)-PPO and negative (positive) for (S)-PPO. The degree of orientation along any axis in the XY plane is identically zero. The general behavior is consistent with previous studies on the enantioselective orientation induced by laser pulses with twisted polarization [21–26]. The scheme presented here, which is based on the shaped picosecond and femtosecond laser pulses, achieves a comparable degree of orientation, resulting in a field-free transient dipole signal of about 0.47 debye corresponding to a degree of orientation $\langle \cos (\theta_{\mu Z}) \rangle \simeq 0.23$. The high degree of alignment generated by the picosecond field (see Fig. 2) serves as a basis for inducing the high degree of enantioselective orientation using the femtosecond laser pulse polarized at angle $\pi/4$ to the polarization direction of the picosecond pulse.

Nowadays, it is still challenging to produce polyatomic molecules exclusively in the rotational ground state in the ex-
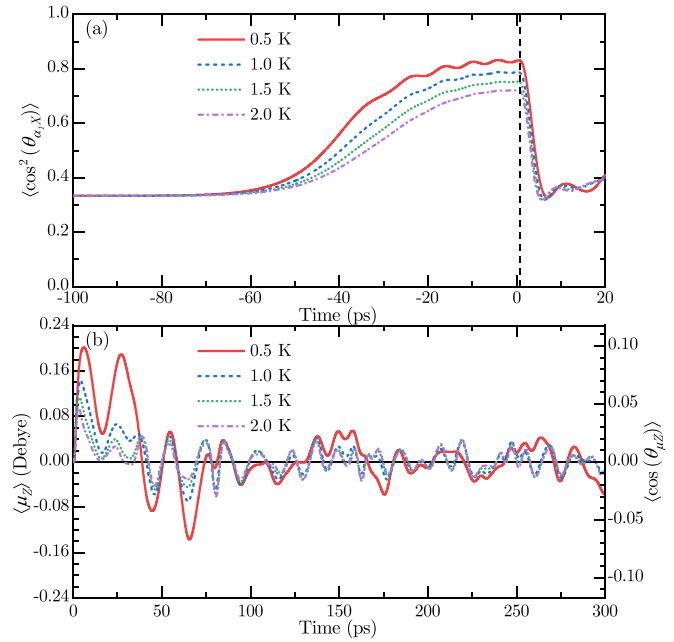

FIG. 4. (a) Quantum-mechanically calculated time-dependent degree of molecular alignment $\langle \cos^2 (\theta_{\alpha_1 X}) \rangle$ for different initial temperatures. Only the shaped picosecond laser pulse is used, and the field parameters used are the same as in Fig. 2. The dashed black line marks the position of $t = 0.77\,\mathrm{ps}$. (b) $\langle \mu_Z \rangle (t)$ of (R)-PPO molecules for different initial temperatures. The laser pulses used are the same as in Fig. 3.

periments. However, a low-temperature distribution or a very narrow distribution of states near the ground state is experimentally available for selection using a so-called state selector [58–60]. Figure 4 depicts the degree of alignment and the degree of enantioselective orientation for different low temperatures. As shown in Fig. 4(a), for the shaped picosecond laser pulse used here, the maximal degree of alignment decreases with the temperature. As a result, the maximal degree of enantioselective orientation following the second femtosecond laser pulse at $t = 0.77\,\mathrm{ps}$ decreases with the temperature [see Fig. 4(b)]. At $T = 0.5\,\mathrm{K}$, a strong transient dipole signal of $\langle \mu_Z \rangle \simeq 0.20\,\mathrm{debye}$ [$\langle \cos (\theta_{\mu Z}) \rangle \simeq 0.099$] can be achieved. A longer and stronger picosecond laser pulse may be useful for inducing a higher degree of alignment for nonzero temperature, e.g., $T = 2\,\mathrm{K}$, which may provide a basis for a higher degree of enantioselective orientation following the second femtosecond pulse. In addition, for nonzero temperature, a stronger second femtosecond laser pulse is expected to induce a higher degree of enantioselective orientation.

IV. QUALITATIVE DESCRIPTION: CLASSICAL MODEL

To understand the origin of the enantioselective orientation shown in Fig. 3 and the role of each of the laser pulses, we resort to a classical model. We consider a collection of classical noninteracting chiral molecules, where each molecule is modeled by a rigid polarizable asymmetric top. The picosecond field prepares a highly aligned molecular ensemble, where the most polarizable molecular α_1 axis points, on average,

along the field polarization direction. To simplify the analysis, we assume that initially (immediately after the end of the picosecond pulse), all the molecular a axes (which are close to the α_1 axis; see Fig. 1) are perfectly aligned along the laboratory X axis, and we take the initial temperature to be 0 K. The aligned molecular ensemble is then excited, at $t = \tau = 0.77$ ps, by a femtosecond laser pulse polarized at angle $\pi/4$ to the X axis [in the XY plane; see Eq. (3)].

Classically, the rotation of a rigid body is described by Euler's equations [61]

$$\mathbf{I}\dot{\mathbf{\Omega}} = (\mathbf{I}\mathbf{\Omega}) \times \mathbf{\Omega} + \mathbf{T}, \tag{4}$$

where $\mathbf{\Omega} = (\Omega_b, \Omega_c, \Omega_a)$ is the angular velocity vector, $\mathbf{I} = \mathrm{diag}(I_b, I_c, I_a)$ is the moment of the inertia tensor, and $\mathbf{T} = (T_b, T_c, T_a)$ is the external torque vector. All the quantities in Eq. (4) are expressed in the molecule-fixed frame of reference using the basis consisting of the three principal axes of inertia, b, c, a. The torque is given by $\mathbf{T} = \boldsymbol{\alpha}\mathbf{E} \times \mathbf{E}$, and it can be obtained by expressing the electric field vector in the molecule-fixed frame. The relation between the laboratory-fixed and molecule-fixed frames is described by $(X, Y, Z)^T = U(\phi, \theta, \chi)(b, c, a)^T$, where the transformation matrix is given by [55]

$$U(A) = \begin{pmatrix} \cos(\phi)\cos(\theta)\cos(\chi) - \sin(\phi)\sin(\chi) & -\cos(\phi)\cos(\theta)\sin(\chi) - \sin(\phi)\cos(\chi) & \cos(\phi)\sin(\theta) \\ \sin(\phi)\cos(\theta)\cos(\chi) + \cos(\phi)\sin(\chi) & -\sin(\phi)\cos(\theta)\sin(\chi) + \cos(\phi)\cos(\chi) & \sin(\phi)\sin(\theta) \\ -\sin(\theta)\cos(\chi) & \sin(\theta)\sin(\chi) & \cos(\theta) \end{pmatrix}. \tag{5}$$

Here, $A = (\phi, \theta, \chi)$ is shorthand notation for the three Euler angles: ϕ and θ are the azimuthal and polar angles defining the orientation of the molecular z axis (associated with the molecular a axis here) in the laboratory-fixed frame, and χ is the additional rotation angle about the z axis (see Fig. 5). The rates of change of the Euler angles are given by [55]

$$\dot{\phi} = \frac{-\Omega_b \cos(\chi) + \Omega_c \sin(\chi)}{\sin(\theta)}, \tag{6a}$$

$$\dot{\theta} = \Omega_b \sin(\chi) + \Omega_c \cos(\chi), \tag{6b}$$

$$\dot{\chi} = \Omega_a - \cos(\theta)\frac{-\Omega_b \cos(\chi) + \Omega_c \sin(\chi)}{\sin(\theta)}. \tag{6c}$$

To describe the ensemble behavior, we use the Monte Carlo approach and consider the dynamics of $N \gg 1$ chiral molecules. For each molecule, we numerically solve a system of differential equations consisting of Eqs. (4) and (6a)–(6c). The N molecules are divided into two groups, I and II. The initial state of the molecules in group I is given by $A(t_0) = (0, \pi/2, \chi_0)$, where χ_0 is uniformly distributed between 0 and

2π, corresponding to the initial state in which the molecular a axes point *along* the laboratory X axis [see Fig. 5(a)]. The initial state of the molecules in group II is defined by $B(t_0) = (\pi, \pi/2, \chi_0)$, such that the molecular a axes point *against* the laboratory X axis [see Fig. 5(b)]. The initial angular velocities are set to $\Omega_i = 0$, $i = b, c, a$, corresponding to a temperature of 0 K.

For convenience, the femtosecond laser pulse is treated as an impulsive excitation, such that the angular velocity just after the pulse is directly proportional to the applied torque, $\Omega_i \propto T_i/I_i$. Considering two molecules, one from each group, in initial states $A(t_0)$ and $B(t_0)$, the torque components in the rotating molecular frame are the same for the two molecules. After averaging over the rapid oscillations of the laser field (the carrier frequency ω is larger than the typical rotation frequency of the molecule by several orders of magnitude) [62], the torque components are given by

$$T_b(\chi_0) = \frac{(E^f)^2}{4}[(\alpha_{cc} - \alpha_{aa})\cos(\chi_0) + \alpha_{bc}\sin(\chi_0) \\ + \alpha_{ac}\sin^2(\chi_0) - \alpha_{ab}\sin(\chi_0)\cos(\chi_0)], \tag{7a}$$

$$T_c(\chi_0) = \frac{(E^f)^2}{4}[(\alpha_{aa} - \alpha_{bb})\sin(\chi_0) - \alpha_{bc}\cos(\chi_0) \\ - \alpha_{ab}\cos^2(\chi_0) + \alpha_{ac}\sin(\chi_0)\cos(\chi_0)], \tag{7b}$$

$$T_a(\chi_0) = \frac{(E^f)^2}{4}[(\alpha_{bb} - \alpha_{cc})\sin(\chi_0)\cos(\chi_0) \\ + \alpha_{bc}\cos(2\chi_0) + \alpha_{ab}\cos(\chi_0) - \alpha_{ac}\sin(\chi_0)]. \tag{7c}$$

Figure 6 shows the classically calculated ensemble average $\langle \mu_Z \rangle(t)$. Here, the initial conditions and the field parameters of the femtosecond pulse are the same as in Fig. 3. Comparing Figs. 3 and 6, it is evident that the simplified classical model qualitatively reproduces the enantioselective orientation. Therefore, in what follows, we analyze the system using the classical model in order to gain physical insight into the qualitative features of the enantioselective orientation.
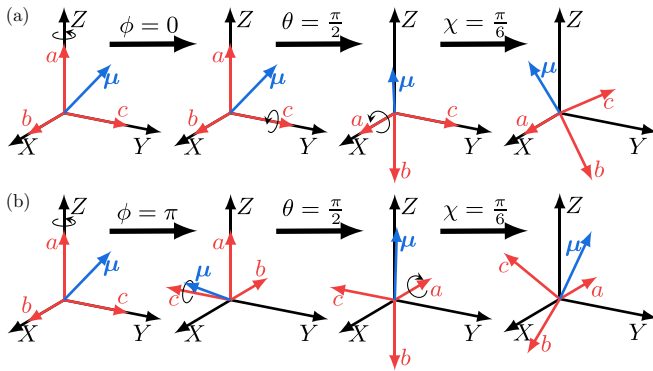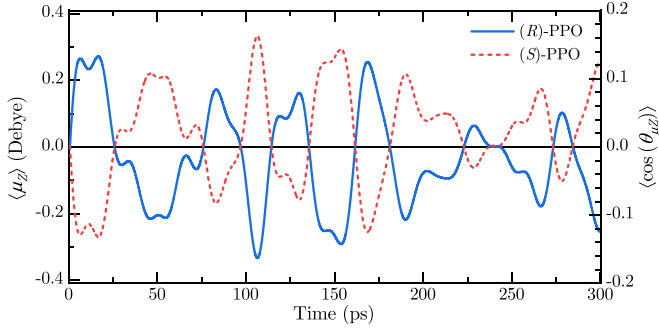

FIG. 5. A set of three Euler rotations (in accordance with the convention of [55]) describing the orientation of the molecule-fixed frame (bca) relative to the laboratory-fixed frame (XYZ) for (a) $A = (0, \pi/2, \pi/6)$ and (b) $B = (\pi, \pi/2, \pi/6)$. The blue arrows represent the dipole moment $\boldsymbol{\mu}$ of a (R)-PPO molecule.

FIG. 6. Classically calculated Z projection of the dipole signal or the degree of orientation. Initially, the molecular a axes are aligned along the X axis, and then the aligned molecules are excited by a femtosecond laser pulse polarized at an angle $\pi/4$ to the X axis. The initial temperature is $0\,\mathrm{K}$. The field parameters of the femtosecond laser pulse are the same as in Fig. 3. $N = 10^7$ molecules are used in the classical simulation.

A. Absence of orientation in the plane of the pulses' polarizations: XY plane

In this section, we consider the orientation along the laser propagation direction and the absence of orientation in any perpendicular direction. Here, we focus on a single enantiomer. The next section addresses the enantioselectivity. As can be seen from Eqs. (6a)–(6c) and (7a)–(7c), the torques (the induced angular velocities) and the rate of change of the Euler angles are independent of ϕ. Accordingly, the initial states $A(t_0)$ and $B(t_0)$ evolve into $A(t) = (\delta\phi, \delta\theta + \pi/2, \delta\chi + \chi_0)$ and $B(t) = (\delta\phi + \pi, \delta\theta + \pi/2, \delta\chi + \chi_0)$, respectively. Here, $\delta\phi$, $\delta\theta$, and $\delta\chi$ are the changes in Euler angles resulting from the rotational dynamics induced by the femtosecond laser pulse kick. Notice the π difference between ϕ angles in $A(t)$ and $B(t)$.

The time-dependent projections of the dipole moment on the laboratory axes can be obtained using the transformation matrix U [see Eq. (5)]:

$$U[A(t)](\mu_b, \mu_c, \mu_a)^T = (\mu_X, \mu_Y, \mu_Z)^T, \qquad (8a)$$

$$U[B(t)](\mu_b, \mu_c, \mu_a)^T = (-\mu_X, -\mu_Y, \mu_Z)^T. \qquad (8b)$$

Equations (8a) and (8b) follow from the fact that the initial π difference in the ϕ angles of A and B is preserved throughout the motion. The same relation can also be found in Fig. 9 below, where we plot the dipole signals as functions of χ_0 for the two molecular groups ($\phi_0 = 0$ and $\phi_0 = \pi$). The dipole moment projections on the X and Y axes are of opposite sign and, when averaged over the entire molecular ensemble (groups I and II), result in zero averaged dipole signal along any direction in the XY plane, including $\langle\mu_X\rangle = \langle\mu_Y\rangle = 0$. In contrast, the dipole moment projections on the Z axis are of the same sign, giving rise to the nonzero ensemble-averaged orientation for chiral molecules, while for nonchiral molecules, $\langle\mu_Z\rangle = 0$ (see below for further details).
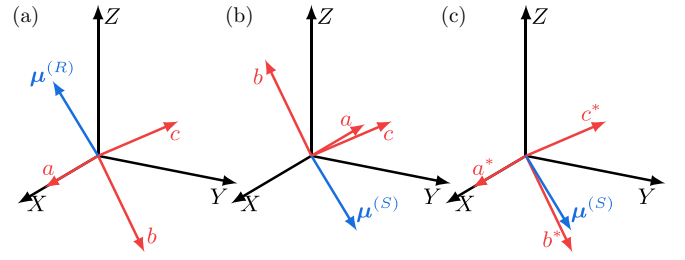

FIG. 7. Two initial orientations of the molecular frame for (a) $A = (0, \pi/2, \chi_0)$ and (b) $B_1 = (\pi, \pi/2, \pi - \chi_0)$. (c) Same as (b) for $B_1^* = (0, \pi/2, \chi_0)$, but in terms of the basis $(b^*, c^*, a^*) = (-b, c, -a)$. Here, $\chi_0 = \pi/6$. $\boldsymbol{\mu}^{(R)}$ and $\boldsymbol{\mu}^{(S)}$ denote dipole moments of (R)- and (S)-PPO molecules, respectively. Note that $\boldsymbol{\mu}^{(S)}$ in (b) and (c) point in the same directions, while $\boldsymbol{\mu}^{(R)}$ in (a) points in the opposite direction.

B. Enantioselective orientation along the laser propagation direction: Z direction

In this section, we consider the implications of chirality on molecular orientation. The two enantiomers are related by a reflection transformation [1]; here, we set the ab plane as the reflection plane. Accordingly, the dipole moment components and the polarizability components of the two enantiomers [(S) and (R)] are related as $\mu_c^{(S)} = -\mu_c^{(R)}$, $\alpha_{ac}^{(S)} = -\alpha_{ac}^{(R)}$, and $\alpha_{bc}^{(S)} = -\alpha_{bc}^{(R)}$. The other components are the same for both enantiomers.

To analyze the enantioselective orientation, we begin with two enantiomers of the propylene oxide molecule, (R)- and (S)-PPO. Initially, the molecular a axes are aligned along the X axis, while the dipole moments of the two enantiomers point in opposite directions (see Fig. 7). Without loss of generality, we consider the initial states $A(t_0) = (0, \pi/2, \chi_0)$ [Fig. 7(a)] and $B_1(t_0) = (\pi, \pi/2, \pi - \chi_0)$ [Fig. 7(b)] for (R)- and (S)-PPO, respectively. For these two states, $\boldsymbol{\mu}^{(R)} = -\boldsymbol{\mu}^{(S)}$. Figure 8 shows the torque components [see Eqs. (7a)–(7c)] as functions of χ_0 for the two enantiomers. The relation between the torque components is given by

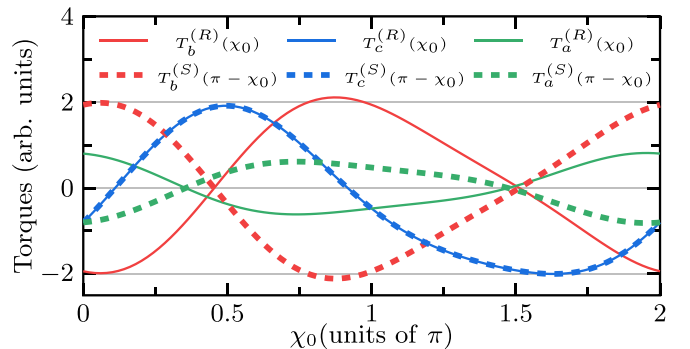$$T_i^{(S)}(\pi - \chi_0) = (-1)^{\delta_{ci}+1} T_i^{(R)}(\chi_0), \ i = b, c, a. \qquad (9)$$

FIG. 8. Torque components [Eqs. (7a)–(7c)] as functions of χ_0 for (R)-PPO (solid lines) and (S)-PPO (dashed lines) molecules with $E^f = 1$.
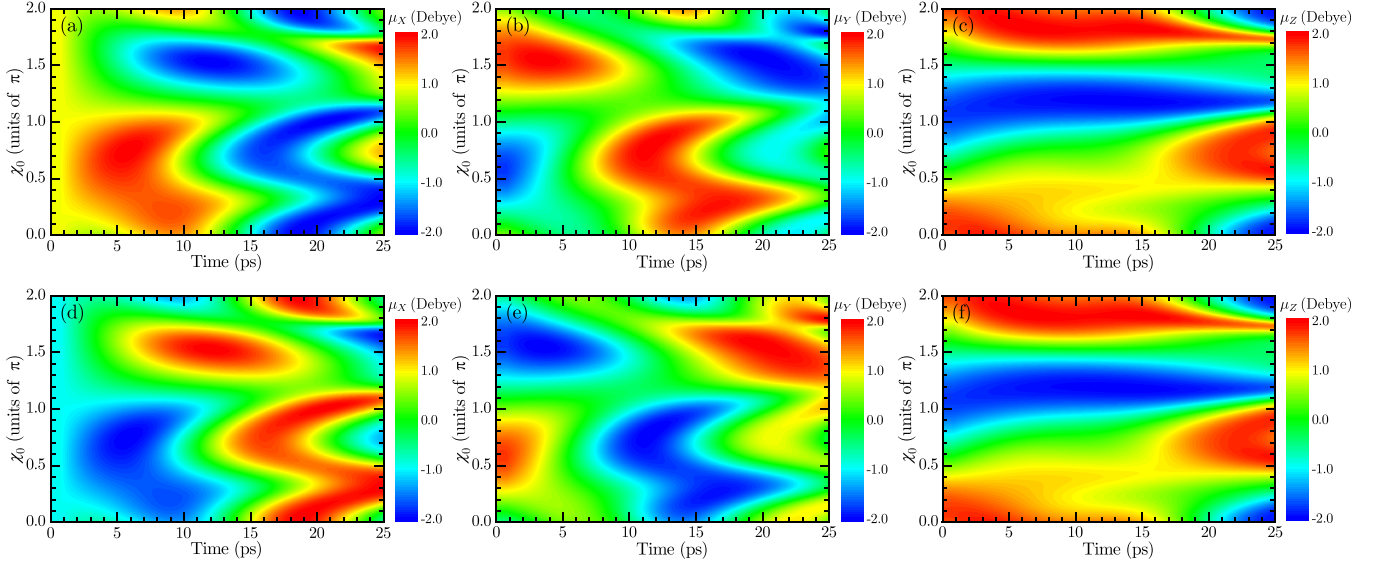
FIG. 9. (a) and (d) X, (b) and (e) Y, and (c) and (f) Z projections of the dipole signal as functions of χ_0 and time for the case of (R)-PPO molecules shown in Fig. 6. (a)–(c) $\phi_0 = 0$, $\theta_0 = \pi/2$. (d)–(f) $\phi_0 = \pi$, $\theta_0 = \pi/2$.

To simplify the comparison of the two enantiomers, we introduce a new basis in the molecular frame of (S)-PPO, consisting of the b^*, c^*, a^* axes, where $(b^*, c^*, a^*) = C_2(c)(b, c, a) = (-b, c, -a)$ and $C_2(c)$ is the twofold rotation about the c axis [55]. In terms of the new basis, the molecular orientation in Fig. 7(b) is given by $B_1^*(t_0) = (0, \pi/2, \chi_0)$ [see Fig. 7(c)]. Note that $B_1^*(t_0) = A(t_0)$. The relation between the torque components of (R)-PPO and (S)-PPO (in terms of the new basis) is

$$T_{i^*}^{(S)}(\chi_0) = T_i^{(R)}(\chi_0) \tag{10}$$

because $T_{i^*}^{(S)}(\chi_0) = (-1)^{\delta_{ci}+1} T_i^{(S)}(\pi - \chi_0)$, $i^* = b^*, c^*, a^*$.

Thus, in this new basis, (b^*, c^*, a^*), the torque components *and* the initial states for both enantiomers in Fig. 7 are the *same*. As a consequence, $B_1^{*(S)}(t) = A^{(R)}(t)$ [see Eqs. (6a)–(6c)]. Moreover, since $(\mu_{b^*}^{(S)}, \mu_{c^*}^{(S)}, \mu_{a^*}^{(S)}) = (-\mu_b^{(S)}, \mu_c^{(S)}, -\mu_a^{(S)}) = -(\mu_b^{(R)}, \mu_c^{(R)}, \mu_a^{(R)})$, we obtain the relations

$$\begin{pmatrix} \mu_X^{(S)}[B_1(t)] \\ \mu_Y^{(S)}[B_1(t)] \\ \mu_Z^{(S)}[B_1(t)] \end{pmatrix} = U[B_1^{(S)}(t)] \begin{pmatrix} \mu_b^{(S)} \\ \mu_c^{(S)} \\ \mu_a^{(S)} \end{pmatrix} = U[B_1^{*(S)}(t)] \begin{pmatrix} \mu_{b^*}^{(S)} \\ \mu_{c^*}^{(S)} \\ \mu_{a^*}^{(S)} \end{pmatrix} = -U[A^{(R)}(t)] \begin{pmatrix} \mu_b^{(R)} \\ \mu_c^{(R)} \\ \mu_a^{(R)} \end{pmatrix} = -\begin{pmatrix} \mu_X^{(R)}[A(t)] \\ \mu_Y^{(R)}[A(t)] \\ \mu_Z^{(R)}[A(t)] \end{pmatrix}, \tag{11}$$

which indicate that the opposite sign between $\boldsymbol{\mu}^{(S)}$ and $\boldsymbol{\mu}^{(R)}$ is preserved throughout the motion (which can also be seen from Figs. 9 and 10). As discussed in Sec. IV A, the ensemble-averaged dipole signal of each enantiomer along any direction in the XY plane is zero. Consequently, the orientation appears in the Z direction, and it is *enantioselective*. Note, however, that in the case of a racemic mixture (which has equal amounts of left- and right-handed enantiomers), the orientation in the Z direction vanishes. Similar and simplified arguments were previously used in [22,23] to explain the enantioselective orientation.

C. Chirality dependence of the orientation along the laser propagation direction: Z direction

In the special case of nonchiral molecules, having a diagonal polarizability tensor, the torque components in Eqs. (7a)–(7c) reduce to

$$T_b(\chi_0) = \frac{(E^f)^2}{4} (\alpha_{cc} - \alpha_{aa}) \cos(\chi_0), \tag{12a}$$

$$T_c(\chi_0) = \frac{(E^f)^2}{4} (\alpha_{aa} - \alpha_{bb}) \sin(\chi_0), \tag{12b}$$

$$T_a(\chi_0) = \frac{(E^f)^2}{4} (\alpha_{bb} - \alpha_{cc}) \sin(\chi_0) \cos(\chi_0). \tag{12c}$$

In contrast to the case of chiral molecules (see Fig. 8), here, the torque components have a well-defined symmetry (symmetric or antisymmetric) about $\chi_0 = n\pi/2$, $n = 0, 1, 2, 3$. For instance,

$$T_i(-\chi_0) = (-1)^{\delta_{bi}+1} T_i(\chi_0), \tag{13a}$$

$$T_i(\pi - \chi_0) = (-1)^{\delta_{ci}+1} T_i(\chi_0), \tag{13b}$$

$$T_i(\pi + \chi_0) = (-1)^{\delta_{ai}+1} T_i(\chi_0). \tag{13c}$$

Note that the relation in Eq. (13b) is the same as in Eq. (9). When the dipole moment projection on the molecular c axis is zero ($\mu_c = 0$), all the expressions from Sec. IV B still apply. Similar to Eq. (11), the relation between the dipole moments corresponding to the initial states of $A(t_0)$ and $B_1(t_0)$ is given
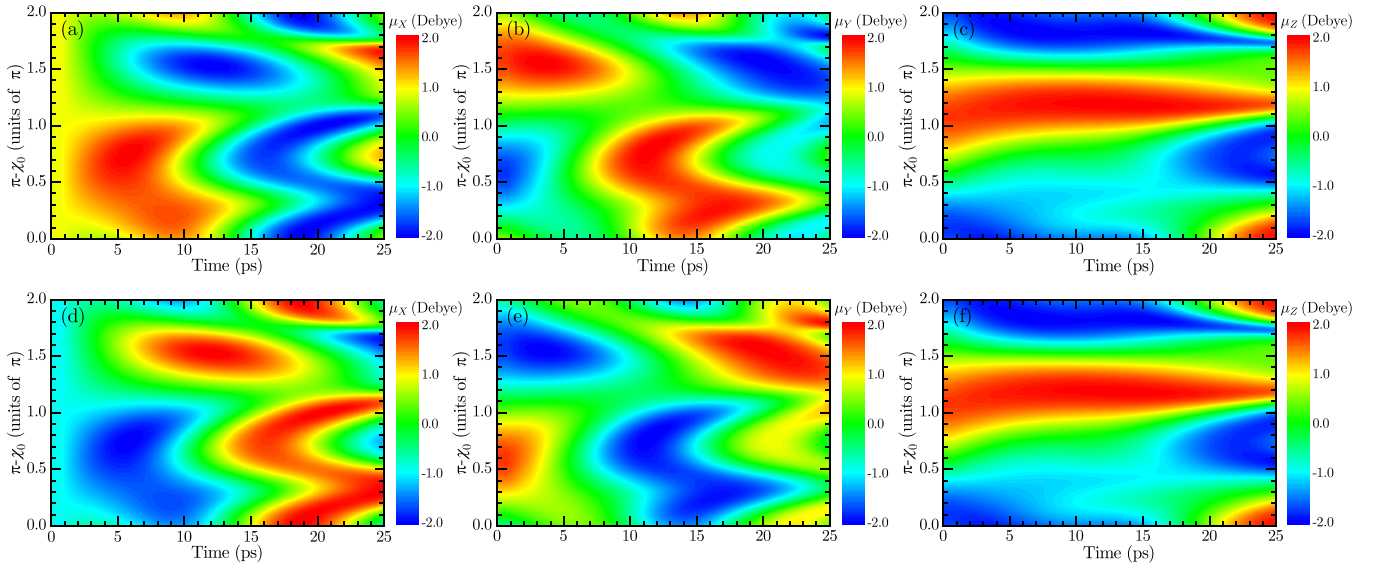
FIG. 10. (a) and (d) X, (b) and (e) Y, and (c) and (f) Z projections of the dipole signal as functions of $\pi - \chi_0$ and time for the case of (S)-PPO molecules shown in Fig. 6. (a)–(c) $\phi_0 = 0$, $\theta_0 = \pi/2$. (d)–(f) $\phi_0 = \pi$, $\theta_0 = \pi/2$.

by

$$\begin{pmatrix} \mu_X[B_1(t)] \\ \mu_Y[B_1(t)] \\ \mu_Z[B_1(t)] \end{pmatrix} = -\begin{pmatrix} \mu_X[A(t)] \\ \mu_Y[A(t)] \\ \mu_Z[A(t)] \end{pmatrix}. \tag{14}$$

Consequently, the ensemble-averaged dipole signal along any laboratory axis is zero, and this includes $\langle \mu_Z \rangle$, the projection along the laser propagation direction. Compared to the two enantiomers in Sec. IV B, the two nonchiral molecules in initial states $A(t_0)$ and $B(t_0)$ are indistinguishable and can be viewed as a mixture containing equal amounts of left- and right-handed enantiomers, leading to the vanishing of the ensemble-averaged orientation. Moreover, notice that $\mu_Z[B_1(t)] = -\mu_Z[A(t)] = -\mu_Z[B(t)]$ [see Eqs. (8a) and (8b)], such that even within each group, $A(t_0)$ and $B(t_0)$, the dipole signal $\langle \mu_Z \rangle$ vanishes. The symmetries of the torque components [see Eqs. (13a) and (13c)] allow repeating the same arguments for molecules in which $\mu_b = 0$ or $\mu_a = 0$.

In contrast, in the case of a single enantiomer of chiral molecules, the torque components do not have symmetry similar to those in Eqs. (13a)–(13c), resulting in the nonzero orientation along the Z axis. This orientation depends on the polarizability tensor being nondiagonal, which is the case for chiral molecules.

D. Roles of the laser pulses

For a collection of isotropically distributed chiral molecules, collinearly polarized one-color laser pulses can induce only molecular alignment and not orientation. Furthermore, orthogonally polarized laser pulses which do not overlap cannot induce orientation either. The reason is that the field-polarizability interaction and the spatial distribution of the molecular ensemble are always symmetric about the axis parallel or perpendicular to the polarization direction.

For the sake of simplicity, we consider an ensemble with the molecular a axes initially aligned along the X axis ($\phi_0 = 0, \pi$, and $\theta_0 = \pi/2$) being excited by a Y-polarized laser pulse. In this case, the torque components denoted as T_i' can be written as

$$T_b'(\chi_0) = -\frac{(E^f)^2}{2}[\alpha_{ab} \sin(\chi_0)\cos(\chi_0) + \alpha_{ac}\cos^2(\chi_0)],$$

$$T_c'(\chi_0) = \frac{(E^f)^2}{2}[\alpha_{ab}\sin^2(\chi_0) + \alpha_{ac}\sin(\chi_0)\cos(\chi_0)],$$

$$T_a'(\chi_0) = \frac{(E^f)^2}{4}[2\alpha_{bc}\cos(2\chi_0) + (\alpha_{bb} - \alpha_{cc})\sin(2\chi_0)].$$

Accordingly, $T_i'(\pi + \chi_0) = T_i'(\chi_0)$, and shortly after the pulse, $\Omega_i'(\pi + \chi_0) = \Omega_i'(\chi_0)$. From Eqs. (6a)–(6c), it follows that for the same θ_0,

$$\delta\theta'(\pi + \chi_0) = -\delta\theta'(\chi_0), \quad \delta\chi'(\pi + \chi_0) = \delta\chi'(\chi_0),$$

such that $\mu_Z'(\pi + \chi_0) = -\mu_Z'(\chi_0)$ [see Eq. (5)]. As a result, because the contributions from the molecules at $\pi + \chi_0$ and χ_0 cancel each other (which can be seen from Fig. 11), the ensemble-averaged dipole signal along the Z axis is zero. Since the torque components depend on only χ_0, the same argument as in Sec. IV A can also be applied, meaning that the dipole signal along any direction in the XY plane vanishes. Thus, there is no orientation in this case.

In contrast, in the case of a pair of delayed crossed-polarized pulses, when the second laser pulse is polarized at an angle ($\neq n\pi/2$, $n = 0, 1, 2, 3$) with respect to the first one, the first pulse effectively breaks the symmetry of spatial distribution about the polarization direction of the second one. Consequently, the induced asymmetric torques [see Eqs. (7a)–(7c)] induce molecular orientation along the direction perpendicular to the polarization of the two exciting pulses. The timescales of polarization twisting and the molecular rotation must be comparable; otherwise, the spatial symmetry about the polarization direction prevails, leading to zero orientation. In our qualitative discussions we did not consider the initial angular velocities, but the conclusions remain valid even when the molecules have finite initial angular velocities.
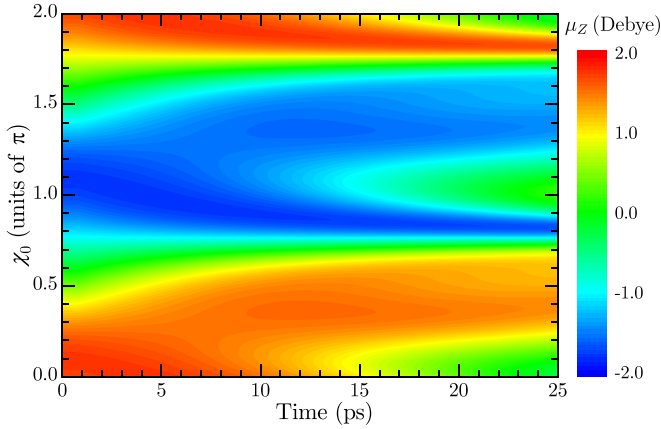
FIG. 11. Z projection of the dipole signal as a function of χ_0 and time for (R)-PPO molecules. The initial conditions and the field parameters of the femtosecond laser pulse are the same as in Fig. 6, except that the femtosecond pulse is polarized along the Y direction. Note that the results for $\phi_0 = 0$ and $\phi_0 = \pi$ are the same.

A similar effect of enantioselective orientation can be achieved using THz pulses with twisted polarization. However, since the THz field couples to the molecular permanent dipole moment, unlike the case of laser pulses, two delayed orthogonally polarized THz pulses can also induce the enantioselective orientation [42].

V. CONCLUSIONS

In this work, we have investigated the enantioselective orientation of chiral molecules excited by a shaped picosecond laser pulse and a delayed femtosecond pulse. We showed that orientation is induced along the laser propagation direction and the sign of orientation is opposite for the two enantiomers. This result is similar to previous works on enantioselective orientation induced by laser pulses with twisted polarization [21–26]. The use of a relatively weak, truncated picosecond pulse to induce alignment may be compared to the use of a strong femtosecond laser pulse because it avoids molecular ionization while still allowing a higher degree of alignment. Another method for achieving a high degree of alignment for a given pulse energy while minimizing molecular ionization is to use a pulse sequence consisting of multiple low-intensity pulses [63–68]. This approach allows the distribution of the energy, which would otherwise be delivered in a single intense pulse, over multiple low-intensity pulses. However, for the optimal degree of alignment, optimization of the sequence parameters is required. Despite the relatively low intensities of the exciting laser pulses, a strong enantioselective orientation (the degree of orientation ≈ 0.23) was demonstrated. The enantioselective orientation may be useful for analyzing the enantiomeric excess and potentially for separating mixtures of enantiomers using inhomogeneous electromagnetic fields [69].

The qualitative features of the effect, including the vanishing orientation in the plane of laser polarizations, the chirality dependence of the enantioselective orientation along the laser propagation direction, and the roles of the two delayed cross-polarized laser pulses, may be understood in terms of the classical model. The shaped picosecond laser pulse prepares a highly aligned molecular ensemble, which is followed by a cross-polarized femtosecond laser pulse. This induces asymmetric torques (depending on the off-diagonal polarizability elements which exist in chiral molecules), resulting in the nonzero orientation along the direction perpendicular to the polarizations of the two exciting pulses. During this process, the orientation along any direction in the plane of pulses' polarizations remains zero. More importantly, although the qualitative argument is based on the transformation properties of the dipole moment and torque between the enantiomers, this is effectively a comparison of the light-matter interaction between the two enantiomers. Therefore, an analysis of the interaction potential, e.g., the interaction between the dipole moment and the terahertz pulses, under the same transformation should lead to the same conclusions.

APPENDIX: TIME-DEPENDENT DIPOLE SIGNAL AS A FUNCTION OF χ_0

Figure 9 depicts the time-dependent dipole signal as a function of χ_0 for the case of (R)-PPO shown in Fig. 6. As can be seen, the dipole signals along the laboratory X and Y axes have opposite signs for $A(t_0) = (0, \pi/2, \chi_0)$ [Figs. 9(a) and 9(b)] and $B(t_0) = (\pi, \pi/2, \chi_0)$ [Figs. 9(d) and 9(e)]. Consequently, the ensemble-averaged dipole signals $\langle \mu_X \rangle$ and $\langle \mu_Y \rangle$ are zero. On the other hand, Figs. 9(c) and 9(f) show that for $A(t)$ and $B(t)$, the Z projections of the dipole signal are the same. These results are consistent with the analysis presented in Sec. IV A.

Figure 10 shows the case of (S)-PPO molecules. The dipole signal of (S)-PPO along the X and Y directions is the same as that of (R)-PPO [$\mu_X^{(S)}(B_1) = \mu_X^{(R)}(B)$ and $\mu_Y^{(S)}(B_1) = \mu_Y^{(R)}(B)$], while $\mu_Z^{(S)}(B_1) = -\mu_Z^{(R)}(B)$. Here, $B = (\pi, \pi/2, \chi_0)$, and $B_1 = (\pi, \pi/2, \pi - \chi_0)$. According to Eq. (11), $\mu_j^{(S)}(B_1) = -\mu_j^{(R)}(A)$, $j = X, Y, Z$. In addition, $\mu_j(B) = (-1)^{\delta_{jZ}+1}\mu_j(A)$ (see Sec. IV A), such that $\mu_j^{(S)}(B_1) = (-1)^{\delta_{jZ}}\mu_j^{(R)}(B)$. The numerical results are consistent with the analysis, and $\mu_Z^{(S)}(B_1) = -\mu_Z^{(R)}(B)$ implies the enantioselective orientation.

Taking the (R)-PPO molecule as an example, we plot $\mu_Z(t)$ as a function of χ_0 in Fig. 11. Initially, $\phi_0 = 0, \pi$ and $\theta_0 = \pi/2$, corresponding to the molecular a axis pointing along or against the laboratory X axis. The initial temperature is 0 K. The femtosecond laser pulse is polarized along the laboratory Y axis. As shown in Fig. 11, $\mu_Z(\pi + \chi_0) = -\mu_Z(\chi_0)$, in agreement with the discussion in Sec. IV D. Consequently, in this case, the ensemble-averaged dipole signal along the Z axis $\langle \mu_Z \rangle$ vanishes.

[1] F. A. Cotton, *Chemical Applications of Group Theory*, 3rd ed. (Wiley, New York, 1990)

[2] L. Pasteur, Sur les relations qui peuvent exister entre la forme cristalline, la composition chimique et le sens de la polarization rotatoire, Ann. Phys. Chem. **24**, 442 (1848).

[3] B. Ritchie, Theory of the angular distribution of photoelectrons ejected from optically active molecules and molecular negative ions, Phys. Rev. A **13**, 1411 (1976).

[4] N. Böwering, T. Lischke, B. Schmidtke, N. Müller, T. Khalil, and U. Heinzmann, Asymmetry in Photoelectron Emission from Chiral Molecules Induced by Circularly Polarized Light, Phys. Rev. Lett. **86**, 1187 (2001).

[5] C. Lux, M. Wollenhaupt, T. Bolze, Q. Liang, J. Köhler, C. Sarpe, and T. Baumert, Circular Dichroism in the Photoelectron Angular Distributions of Camphor and Fenchone from Multiphoton Ionization with Femtosecond Laser Pulses, Angew. Chem., Int. Ed. **51**, 5001 (2012).

[6] S. Beaulieu, A. Comby, A. Clergerie, J. Caillat, D. Descamps, N. Dudovich, B. Fabre, R. Géneaux, F. Légaré, S. Petit, B. Pons, G. Porat, T. Ruchon, R. Taïeb, V. Blanchet, and Y. Mairesse, Attosecond-resolved photoionization of chiral molecules, Science **358**, 1288 (2017).

[7] S. Beaulieu, A. Comby, D. Descamps, B. Fabre, G. A. Garcia, R. Géneaux, A. G. Harvey, F. Légaré, Z. Mašín, L. Nahon, A. F. Ordonez, S. Petit, B. Pons, Y. Mairesse, O. Smirnova, and V. Blanchet, Photoexcitation circular dichroism in chiral molecules, Nat. Phys. **14**, 484 (2018).

[8] D. Patterson, M. Schnell, and J. M. Doyle, Enantiomer-specific detection of chiral molecules via microwave spectroscopy, Nature (London) **497**, 475 (2013).

[9] D. Patterson and J. M. Doyle, Sensitive Chiral Analysis via Microwave Three-Wave Mixing, Phys. Rev. Lett. **111**, 023008 (2013).

[10] D. Patterson and M. Schnell, New studies on molecular chirality in the gas phase: Enantiomer differentiation and determination of enantiomeric excess, Phys. Chem. Chem. Phys. **16**, 11114 (2014).

[11] V. A. Shubert, D. Schmitz, and M. Schnell, Enantiomer-sensitive spectroscopy and mixture analysis of chiral molecules containing two stereogenic centers – microwave three-wave mixing of menthone, J. Mol. Spectrosc. **300**, 31 (2014).

[12] K. K. Lehmann, Theory of enantiomer-specific microwave spectroscopy, in *Frontiers and Advances in Molecular Spectroscopy* (Elsevier, Amsterdam, 2018), pp. 713–743.

[13] C. Ye, Q. Zhang, and Y. Li, Real single-loop cyclic three-level configuration of chiral molecules, Phys. Rev. A **98**, 063401 (2018).

[14] C. Ye, Q. Zhang, Y.-Y. Chen, and Y. Li, Determination of enantiomeric excess with chirality-dependent ac Stark effects in cyclic three-level models, Phys. Rev. A **100**, 033411 (2019).

[15] M. Leibscher, T. F. Giesen, and C. P. Koch, Principles of enantio-selective excitation in three-wave mixing spectroscopy of chiral molecules, J. Chem. Phys. **151**, 014302 (2019).

[16] M. Pitzer, M. Kunitski, A. S. Johnson, T. Jahnke, H. Sann, F. Sturm, L. Ph. H. Schmidt, H. Schmidt-Böcking, R. Dörner, J. Stohner, J. Kiedrowski, M. Reggelin, S. Marquardt, A. Schießer, R. Berger, and M. S. Schöffler, Direct determination of absolute molecular stereochemistry in gas phase by Coulomb explosion imaging, Science **341**, 1096 (2013).

[17] P. Herwig, K. Zawatzky, M. Grieser, O. Heber, B. Jordon-Thaden, C. Krantz, O. Novotný, R. Repnow, V. Schurig, D. Schwalm, Z. Vager, A. Wolf, O. Trapp, and H. Kreckel, Imaging the absolute configuration of a chiral epoxide in the gas phase, Science **342**, 1084 (2013).

[18] K. Fehre, S. Eckart, M. Kunitski, M. Pitzer, S. Zeller, C. Janke, D. Trabert, J. Rist, M. Weller, A. Hartung, L. Ph. H. Schmidt, T. Jahnke, R. Berger, R. Dörner, and M. S. Schöffler, Enantioselective fragmentation of an achiral molecule in a strong laser field, Sci. Adv. **5**, eaau7923 (2019).

[19] R. Cireasa, A. E. Boguslavskiy, B. Pons, M. C. H. Wong, D. Descamps, S. Petit, H. Ruf, N. Thiré, A. Ferré, J. Suarez, J. Higuet, B. E. Schmidt, A. F. Alharbi, F. Légaré, V. Blanchet, B. Fabre, S. Patchkovskii, O. Smirnova, Y. Mairesse, and V. R. Bhardwaj, Probing molecular chirality on a sub-femtosecond timescale, Nat. Phys. **11**, 654 (2015).

[20] K. Banerjee-Ghosh, O. Ben Dor, F. Tassinari, E. Capua, S. Yochelis, A. Capua, S.-H. Yang, S. S. P. Parkin, S. Sarkar, L. Kronik, L. T. Baczewski, R. Naaman, and Y. Paltiel, Separation of enantiomers by their enantiospecific interaction with achiral magnetic substrates, Science **360**, 1331 (2018).

[21] A. Yachmenev and S. N. Yurchenko, Detecting Chirality in Molecules by Linearly Polarized Laser Fields, Phys. Rev. Lett. **117**, 033001 (2016).

[22] E. Gershnabel and I. Sh. Averbukh, Orienting Asymmetric Molecules by Laser Fields with Twisted Polarization, Phys. Rev. Lett. **120**, 083204 (2018).

[23] I. Tutunnikov, E. Gershnabel, S. Gold, and I. Sh. Averbukh, Selective orientation of chiral molecules by laser fields with twisted polarization, J. Phys. Chem. Lett. **9**, 1105 (2018).

[24] A. A. Milner, J. A. M. Fordyce, I. MacPhail-Bartley, W. Wasserman, V. Milner, I. Tutunnikov, and I. Sh. Averbukh, Controlled Enantioselective Orientation of Chiral Molecules with an Optical Centrifuge, Phys. Rev. Lett. **122**, 223201 (2019).

[25] I. Tutunnikov, J. Floß, E. Gershnabel, P. Brumer, and I. Sh. Averbukh, Laser-induced persistent orientation of chiral molecules, Phys. Rev. A **100**, 043406 (2019).

[26] I. Tutunnikov, J. Floß, E. Gershnabel, P. Brumer, I. Sh. Averbukh, A. A. Milner, and V. Milner, Observation of persistent orientation of chiral molecules by a laser field with twisted polarization, Phys. Rev. A **101**, 021403(R) (2020).

[27] S. Fleischer, Y. Khodorkovsky, Y. Prior, and I. Sh. Averbukh, Controlling the sense of molecular rotation, New J. Phys. **11**, 105039 (2009).

[28] K. Kitano, H. Hasegawa, and Y. Ohshima, Ultrafast Angular Momentum Orientation by Linearly Polarized Laser Fields, Phys. Rev. Lett. **103**, 223002 (2009).

[29] Y. Khodorkovsky, K. Kitano, H. Hasegawa, Y. Ohshima, and I. Sh. Averbukh, Controlling the sense of molecular rotation: Classical versus quantum analysis, Phys. Rev. A **83**, 023423 (2011).

[30] J. Karczmarek, J. Wright, P. Corkum, and M. Ivanov, Optical Centrifuge for Molecules, Phys. Rev. Lett. **82**, 3420 (1999).

[31] D. M. Villeneuve, S. A. Aseyev, P. Dietrich, M. Spanner, M. Yu. Ivanov, and P. B. Corkum, Forced Molecular Rotation in an Optical Centrifuge, Phys. Rev. Lett. **85**, 542 (2000).

[32] L. Yuan, S. W. Teitelbaum, A. Robinson, and A. S. Mullin, Dynamics of molecules in extreme rotational states, Proc. Natl. Acad. Sci. USA **108**, 6872 (2011).

[33] A. Korobenko, A. A. Milner, and V. Milner, Direct Observation, Study, and Control of Molecular Superrotors, Phys. Rev. Lett. **112**, 113004 (2014).

[34] A. Korobenko, Control of molecular rotation with an optical centrifuge, J. Phys. B **51**, 203001 (2018).

[35] S. Zhdanovich, A. A. Milner, C. Bloomquist, J. Floß, I. Sh. Averbukh, J. W. Hepburn, and V. Milner, Control of Molecular Rotation with a Chiral Train of Ultrashort Pulses, Phys. Rev. Lett. **107**, 243004 (2011).

[36] J. Floß and I. Sh. Averbukh, Molecular spinning by a chiral train of short laser pulses, Phys. Rev. A **86**, 063414 (2012).

[37] Y. Kida, S.-I. Zaitsu, and T. Imasaka, Stimulated rotational Raman scattering by a polarization-modulated femtosecond pulse, Phys. Rev. A **77**, 063802 (2008).

[38] Y. Kida, S.-I. Zaitsu, and T. Imasaka, Coherent molecular rotations induced by a femtosecond pulse consisting of two orthogonally polarized pulses, Phys. Rev. A **80**, 021805(R) (2009).

[39] G. Karras, M. Ndong, E. Hertz, D. Sugny, F. Billard, B. Lavorel, and O. Faucher, Polarization Shaping for Unidirectional Rotational Motion of Molecules, Phys. Rev. Lett. **114**, 103001 (2015).

[40] E. Prost, H. Zhang, E. Hertz, F. Billard, B. Lavorel, P. Bejot, J. Zyss, I. Sh. Averbukh, and O. Faucher, Third-order-harmonic generation in coherently spinning molecules, Phys. Rev. A **96**, 043418 (2017).

[41] K. Mizuse, N. Sakamoto, R. Fujimoto, and Y. Ohshima, Direct imaging of direction-controlled molecular rotational wave packets created by a polarization-skewed double-pulse, Phys. Chem. Chem. Phys. **22**, 10853 (2020).

[42] I. Tutunnikov, L. Xu, R. W. Field, K. A. Nelson, Y. Prior, and I. Sh. Averbukh, Enantioselective orientation of chiral molecules induced by terahertz pulses with twisted polarization, Phys. Rev. Research **3**, 013249 (2021).

[43] N. Takemoto and K. Yamanouchi, Fixing chiral molecules in space by intense two-color phase-locked laser fields, Chem. Phys. Lett. **451**, 1 (2008).

[44] L. Xu, I. Tutunnikov, Y. Prior, and I. Sh. Averbukh, Three dimensional orientation of small polyatomic molecules excited by two-color femtosecond pulses, J. Phys. B **54**, 164003 (2021).

[45] O. Korech, U. Steinitz, R. J. Gordon, I. Sh. Averbukh, and Y. Prior, Observing molecular spinning via the rotational doppler effect, Nat. Photonics **7**, 711 (2013).

[46] K. Mizuse, K. Kitano, H. Hasegawa, and Y. Ohshima, Quantum unidirectional rotation directly imaged with molecules, Sci. Adv. **1**, e1400185 (2015).

[47] K. Lin, Q. Song, X. Gong, Q. Ji, H. Pan, J. Ding, H. Zeng, and J. Wu, Visualizing molecular unidirectional rotation, Phys. Rev. A **92**, 013410 (2015).

[48] T. Seideman, On the dynamics of rotationally broad, spatially aligned wave packets, J. Chem. Phys. **115**, 5965 (2001).

[49] J. G. Underwood, M. Spanner, M. Yu. Ivanov, J. Mottershead, B. J. Sussman, and A. Stolow, Switched Wave Packets: A Route to Nonperturbative Quantum Control, Phys. Rev. Lett. **90**, 223001 (2003).

[50] J. G. Underwood, B. J. Sussman, and A. Stolow, Field-Free Three Dimensional Molecular Axis Alignment, Phys. Rev. Lett. **94**, 143002 (2005).

[51] A. Goban, S. Minemoto, and H. Sakai, Laser-Field-Free Molecular Orientation, Phys. Rev. Lett. **101**, 013001 (2008).

[52] A. S. Chatterley, C. Schouder, L. Christiansen, B. Shepperson, M. H. Rasmussen, and H. Stapelfeldt, Long-lasting field-free alignment of large molecules inside helium nanodroplets, Nat. Commun. **10**, 133 (2019).

[53] R. V. Krems, *Molecules in Electromagnetic Fields: From Ultracold Physics to Controlled Chemistry* (Wiley, New York, 2018).

[54] C. P. Koch, M. Lemeshko, and D. Sugny, Quantum control of molecular rotation, Rev. Mod. Phys. **91**, 035005 (2019).

[55] R. N. Zare, *Angular Momentum: Understanding Spatial Aspects in Chemistry and Physics* (Wiley, New York, 1988).

[56] R. B. Sidje, Expokit: A software package for computing matrix exponentials, ACM Trans. Math. Software **24**, 130 (1998).

[57] M. J. Frisch *et al.*, GAUSSIAN 16, revision A.03, Gaussian Inc. Wallingford, CT, 2016.

[58] F. Filsinger, J. Küpperr, G. Meijer, L. Holmegaard, J. H. Nielsen, I. Nevo, J. L. Hansen, and H. Stapelfeldt, Quantum-state selection, alignment, and orientation of large molecules using static electric and laser fields, J. Chem. Phys. **131**, 064309 (2009).

[59] L. Holmegaard, J. H. Nielsen, I. Nevo, H. Stapelfeldt, F. Filsinger, J. Küpper, and G. Meijer, Laser-Induced Alignment and Orientation of Quantum-State-Selected Large Molecules, Phys. Rev. Lett. **102**, 023001 (2009).

[60] M. M. Hossain, X. Zhang, S. Minemoto, and H. Sakai, Stronger orientation of state-selected OCS molecules with relative-delay-adjusted nanosecond two-color laser pulses, J. Chem. Phys. **156**, 041101 (2022).

[61] H. Goldstein, C. Poole, and J. Safko, *Classical Mechanics* (Addison Wesley, San Francisco, 2002).

[62] B. J. Sussman, Five ways to the nonresonant dynamic Stark effect, Am. J. Phys. **79**, 477 (2011).

[63] I. Sh. Averbukh and R. Arvieu, Angular Focusing, Squeezing, and Rainbow Formation in a Strongly Driven Quantum Rotor, Phys. Rev. Lett. **87**, 163601 (2001).

[64] M. Leibscher, I. Sh. Averbukh, and H. Rabitz, Molecular Alignment by Trains of Short Laser Pulses, Phys. Rev. Lett. **90**, 213001 (2003).

[65] M. Leibscher, I. Sh. Averbukh, and H. Rabitz, Enhanced molecular alignment by short laser pulses, Phys. Rev. A **69**, 013402 (2004).

[66] K. F. Lee, I. V. Litvinyuk, P. W. Dooley, M. Spanner, D. M. Villeneuve, and P. B. Corkum, Two-pulse alignment of molecules, J. Phys. B **37**, L43 (2004).

[67] C. Z. Bisgaard, M. D. Poulsen, E. Péronne, S. S. Viftrup, and H. Stapelfeldt, Observation of Enhanced Field-Free Molecular Alignment by Two Laser Pulses, Phys. Rev. Lett. **92**, 173004 (2004).

[68] D. Pinkham, K. E. Mooney, and R. R. Jones, Optimizing dynamic alignment in room temperature CO, Phys. Rev. A **75**, 013422 (2007).

[69] A. Yachmenev, J. Onvlee, E. Zak, A. Owens, and J. Küpper, Field-Induced Diastereomers for Chiral Separation, Phys. Rev. Lett. **123**, 243202 (2019).